Journal of Power Sources 267 (2014) 753–759

Contents lists available at ScienceDirect

Journal of Power Sources

journal homepage: www.elsevier.com/locate/jpowsour

Controlling the redox reaction at the interface between sealing glasses and Cr-containing interconnect: Effect of competitive reaction

Shunrun Chen [a], Jianxin Lin [a], Hsiwen Yang [b], Dian Tang [a], Teng Zhang [a, *]

[a] College of Materials Science and Engineering, Fuzhou University, Fuzhou, Fujian 350108, China
[b] Department of Materials Science and Engineering, National United University, Miao-Li 36003, Taiwan, China

HIGHLIGHTS

- The competitive reaction reduces the glass/metal interfacial reaction.
- The reaction also results in a stable Mn–Cr oxide scale at the interface.
- The Mn–Cr oxide scale acts as diffusion barrier at the glass/metal interface.

ARTICLE INFO

Article history:
Received 19 January 2014
Received in revised form
1 June 2014
Accepted 2 June 2014
Available online 10 June 2014

Keywords:
Solid Oxide Fuel Cells
Interfacial reaction
Sealing glass
Valence state
Glass structure

ABSTRACT

In this paper, MnO_2 is added to $CaO–SrO–B_2O_3–SiO_2$ sealing system to control the redox glass/metal interfacial reaction in Solid Oxide Fuel Cells. The effect of MnO_2 dopant on the valance states of Mn ions in glasses, the glass structure and glass/metal interfacial reaction is systematically investigated. The quenched glasses contain Mn^{2+} ion only; whereas, the Mn^{3+} content in glasses, held at 600 °C for 9 h, increases with increasing MnO_2 dopant. The good bondage can be observed at the interfaces between Crofer 22APU and glass containing 6 mol % MnO_2, held at 700 °C for 500 h. The competitive reaction reduces the redox chromate formation by consuming the oxygen at the glass/metal interface. In addition, the competitive reaction results in the formation of a continuous Mn–Cr oxide scale at the glass/metal interface, which is helpful for reducing the further diffusion of Cr from metallic interconnect to glass.

1. Introduction

The direct operation of Solid Oxide Fuel Cells (SOFCs) on hydrocarbon fuels has attracted increasing attention in the last decade, due to the large amount of hydrocarbons as well as the highest conversion efficiency of SOFC among all types of fuel cells [1–3].

However, the long-term operation of SOFCs still faces many challenges, for example, the coke formation as well as the interfacial reaction between sealing glasses and other Solid Oxide Fuel Cell (SOFC) components. In particular, the chromate formation at the interface between sealing glasses and Cr-containing interconnect often leads to the generation of thermal stress and subsequently the physical separation of sealing glass from metallic interconnect [4–8].

Many efforts have been made on the modification of interconnects, including pre-oxidation [9–13], aluminizing [14,15] and protective coatings [16–21], in order to hinder the diffusion of Cr from the interconnect to the glass. However, few works on the improvement of the chemical compatibility of sealing glasses have been reported in literature, because of the difficulty in the quantitative analysis of the reaction in complex fixture of SOFCs. A recent work of our group has clearly demonstrated the effect of crystallization process on the interfacial reaction [22] using a quantitative approach developed by ourselves [23].

Considering the redox characteristic of the interfacial reaction (*e.g.*, $SrO + 0.5Cr_2O_3 + 0.75O_2 = SrCrO_4$) [7], ions with different valence states, such as Mn, Fe and Ce, in glasses might act as a competitive reaction for the interfacial reaction, by consuming the oxygen at the triple-phase boundary (TPB). In this paper, MnO_2 is added gradually, from 2 to 10 mol %, to a representative Sr-containing borosilicate sealing glass. Attention has been focused on the valence states of Mn ions in glasses and its effect on the glass/metal interfacial reaction to provide useful information on the control of redox-type interfacial reaction.

* Corresponding author. Tel.: +86 591 22866540; fax: +86 591 22866537.
E-mail address: teng_zhang@fzu.edu.cn (T. Zhang).

http://dx.doi.org/10.1016/j.jpowsour.2014.06.004
0378-7753/

Table 1
Nominal compositions (in mol %) of glasses.

Sample ID	SrO	CaO	B_2O_3	SiO_2	MnO_2	B/Si	Sr/Ca	Mn/Si
Glass#M1	25.48	25.48	7.84	39.2	2	0.40	1.00	0.05
Glass#M2	24.96	24.96	7.68	38.4	4	0.40	1.00	0.10
Glass#M3	24.44	24.44	7.52	37.6	6	0.40	1.00	0.16
Glass#M4	23.92	23.92	7.36	36.8	8	0.40	1.00	0.21
Glass#M5	23.4	23.4	7.2	36	10	0.40	1.00	0.28

2. Experimental

A 50-g sample of each glass was prepared by melting a homogeneous mixture of reagent grade alkaline earth carbonates, boric acid, and various oxides in a platinum crucible in air at 1500 °C for one hour. The nominal compositions of glasses (mol %) are shown in Table 1. Some of the melt was poured into stainless steel mold to obtain cylindrical shaped glass specimens (25 mm length and 6 mm diameter) and the rest of the melt was quenched on a steel plate. Glass powders were then crushed and sieved to a particle size of 45–53 μm. The final compositions of quenched glasses measured by XPS are shown in Table 2.

Raman spectra of quenched glasses powders were collected in 200–1600 cm^{-1} wave number range by Raman spectrometer (Renishaw invia). The light source was 514.5 nm argon laser with 10 s of exposure time. The spectra were analyzed by Gaussian fitting with Peak-Fit4.1 software. In addition, the crystalline phases in glass–ceramics powders, held at 700 °C for 100 h, were identified by X-ray diffraction (XDS 2000, Scintag, Inc.).

The onset crystallization temperature (T_c) of glass powders was determined using differential scanning calorimetry (SDTQ600, TA, Inc.) at a heating rate of 10 °C min^{-1}. The dilatometric characteristics of quenched glasses, including the coefficient of thermal expansion (CTE, between 200 and 600 °C), glass transition temperature (T_g) and dilatometric softening temperature (T_d), were determined by dilatometer (DIL402C, NETZSCH, Inc.) at 10 °C min^{-1} in air. Thermal properties of glasses, including T_c, T_g, T_d and CTE, are summarized in Table 4.

A ~10 mg mixture of glass and 10 weight % Cr_2O_3 powders was reacted in an alumina boat in air for different times. The reaction temperature was chosen to be 600 °C to exclude the effects of crystallization and softening processes (in Fig. 1 and Table 4). The reaction product was dissolved into ~50 ml of deionized water and the absorption spectra were recorded using the UV–vis Spectrometer (Optima 2000 DV, Perkin Elmer, Inc.). The fraction of Cr^{6+} was then calculated by fitting the measured absorption to the calibration curve. The detailed procedure of this analysis has also been discussed elsewhere [23].

The emission spectra of Mn^{2+} and Mn^{3+} ions in quenched glass powders were collected using the spectorfluorometer (Fluoromax-4, HORIBA Scientific, Inc.), after excitation at 420 nm and 490 nm, respectively. The valence states of Mn ions in glasses, held at 600 °C for 9 h, were determined by X-ray photoelectron spectroscopy (ESCALAB 250, Thermo Scientific, Inc.) using a monochromatic Al Kα source (10 mA, 15 kV).

The glasses were bonded to Crofer 22APU substrates and the interfacial reactions were characterized. Glass pastes were prepared by mixing ~50 mg glass powder (45–53 μm) with ~50 μl acetone. The pastes were applied to the ultrasonically-cleaned surfaces of Crofer 22APU. The coated samples were subsequently held in air at 700 °C for 100 h. The glass/metal sealing couples were polished using SiC paper from 320 to 1200 grit, and then finished using an alumina suspension (3 μm). The polished samples were analyzed using field emission scanning electron microscopy (Supra-55, Zeiss, Inc.) and energy dispersive analysis by X-rays (X-Max, OXFORD instruments, Inc.).

Table 2
Final compositions (in mol %) of quenched glasses measured by XPS.

Sample ID	CaO	SrO	B_2O_3	SiO_2	MnO_2	B/Si	Sr/Ca	Mn/Si
Glass#M1	26.0	25.6	7.3	39.6	1.5	0.40	0.99	0.04
Glass#M3	23.9	24.3	7.0	39.1	5.7	0.40	1.01	0.14
Glass#M5	23.5	24.0	6.7	36	9.8	0.41	1.02	0.27

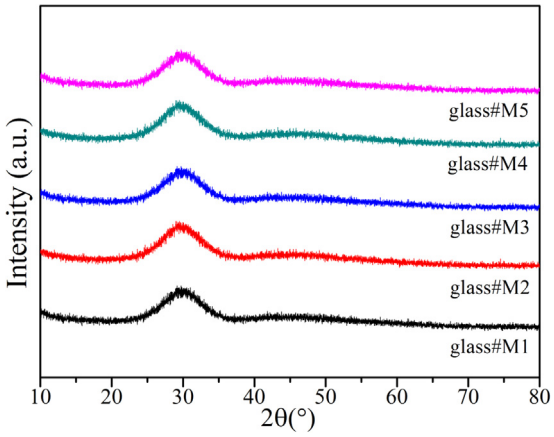

Fig. 1. XRD spectra of glasses held at 600 °C for 9 h.

3. Results and discussion

3.1. Valance states of Mn ions in glasses

Fig. 2 shows the photoluminescence spectrum of quenched glass#M5. It is clear that peaks corresponding for Mn^{2+} ion can be observed after excitation at 420 nm; whereas, no peak can be detected after excitation at 490 nm, indicating the absence of Mn^{3+} ion in present work. It is well known that the valance states of Mn ions depend strongly on the manganese content in glasses [24]. The Mn^{2+} ion is common in quenched glasses, while the Mn^{3+} ion can only be detected in glasses with great Mn content, *e.g.*, more than 10 mol % [25,26]. Therefore, the quenched glasses in present work contain Mn^{2+} ion only.

To clarify the change in valance states of Mn ions during the interfacial reaction, the XPS analysis was also conducted on the

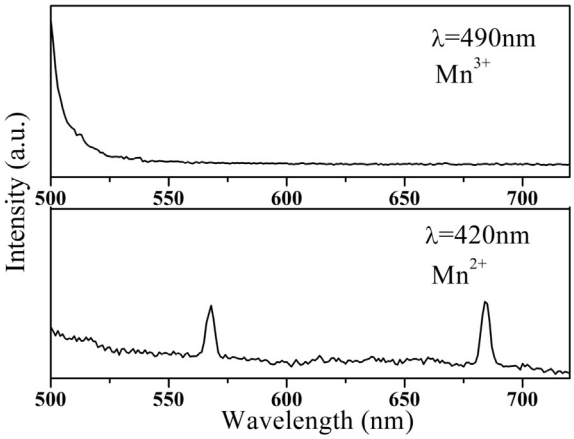

Fig. 2. Photoluminescence spectrum of quenched glass#M5.

glasses treated under the same condition of interfacial reaction between glass and Cr_2O_3 powders. Fig. 3 shows the Mn 2p spectra of glasses with different MnO_2 dopant, held at 600 °C for 9 h. Because of similar binding energies of different Mn ions, the deconvoluted peaks are generally needed to distinguish Mn ions with different valance states [27,28]. The Mn 2p spectra of glasses in present work can be deconvoluted into five peaks, *i.e.*, 640.8, 641.9, 643.1, 644.6 and 646.2 eV, according to the process described elsewhere [29]. The relative amount of Mn^{3+} ion of glasses increases from 72% for glass#M1 to 77% for glass#M3 and to 88% for glass#M5.

In addition, the Gibbs free energy of the reaction from Mn^{2+} to Mn^{3+} in glasses with different MnO_2 dopant was calculated as a function of temperature. The activity of MnO is simplified to be its molar fraction in glasses in present work, assuming the glass is ideal solution. As shown in Fig. 4, the Gibbs free energy of the reaction, *i.e.*, $2MnO + 0.5O_2 = Mn_2O_3$, decreases with increasing MnO_2 dopant in glasses. For example, the Gibbs free energy of the reaction at 873 K in air decreases from −142.8 kJ mol^{-1} for glass#M1 to −150.4 kJ mol^{-1} for glass#M3 and to −153.0 kJ mol^{-1} for glass#M5, consistent with the quantitative results of XPS (in Fig. 3).

3.2. Glass structure and thermal properties of glasses

Shown in Fig. 5 are the Raman spectra of quenched glasses. The Raman spectra generally can be divided into four regions, *i.e.*, below 400, 550–800, 800–1300 and 1300–1600 cm^{-1} [30–32]. In particular, the vibration modes in the wave number ranging from 800 to 1300 cm^{-1} are mainly associated with the Si–O stretch modes in Si tetrahedral units [33,34]. Fig. 5(b)–(d) shows the deconvoluted Raman spectra in the region of 1300–1600 cm^{-1} for glass#M1, glass#M3 and glass#M5, respectively. The fractions of different $[SiO_4]$ units in quenched glasses can be calculated by comparing the integrated areas of deconvoluted peaks, as shown in Table 3. The fraction of bridging oxygen in Si tetrahedral decreases from 45% for glass#M1 to 41% for glass#M3 and to 38% for glass#M5. In addition, Q^3/Q^2 ratio is often regarded as an index for the degree of polymerization [35–37]. The Q^3/Q^2 ratio in present work decreases from 0.21 for glass#M1 to 0.12 for glass#M3 and to 0.06 for glass#M5.

On the other hand, the O1s XPS curves are often deconvoluted into two peaks with different binding energies, *i.e.*, non-bridging oxygen and bridging oxygen, respectively. The fraction of bridging oxygen can be calculated by comparing the integrated areas of two peaks and thus provides quantitative information on the overall network connectivity of glasses [38,39]. Fig. 6 shows the O1s spectra of quenched glasses. It is worth noting that the fraction of bridging oxygen in glasses decreases from 81% for glass#M1 to 78% for glass#M3 and to 73% for glass#M5. This also

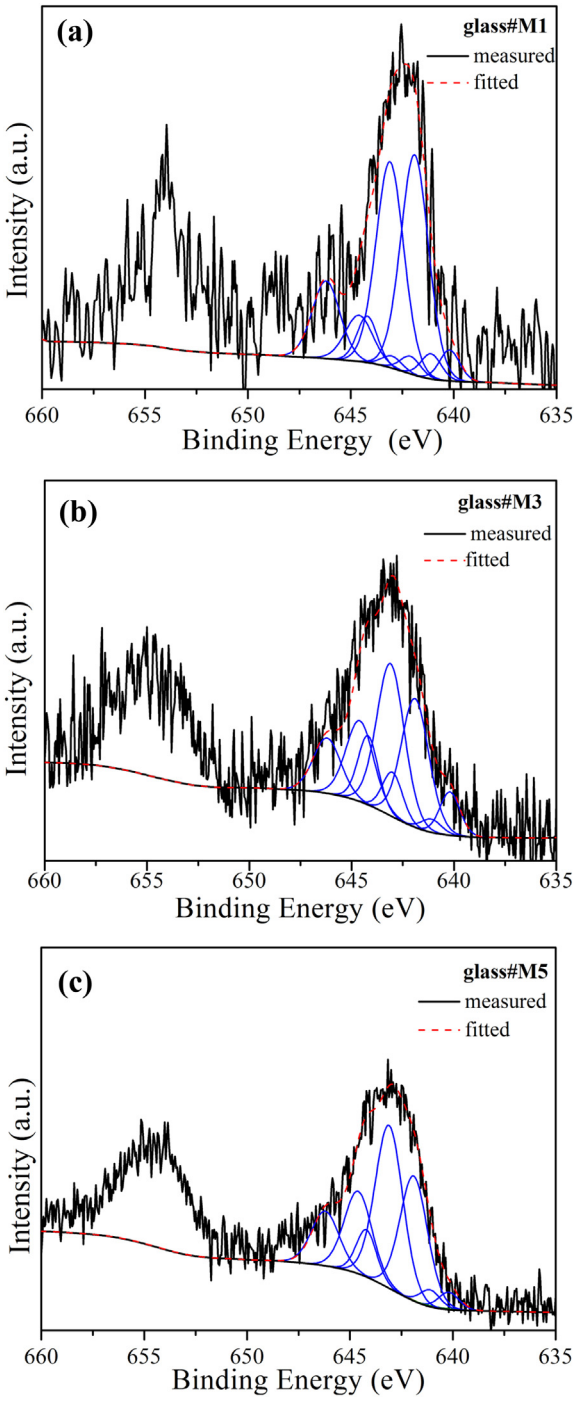

Fig. 3. Mn 2p spectra of sealing glasses held at 600 °C for 9 h, for (a) glass#M1, (b) glass#M3, and (c) glass#M5.

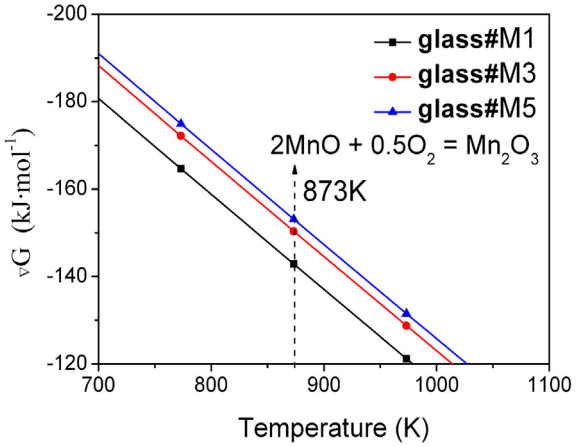

Fig. 4. The Gibbs free energies of the reaction ($2MnO + 0.5O_2 = Mn_2O_3$) in sealing glasses for glass#M1, glass#M3 and glass#M5.

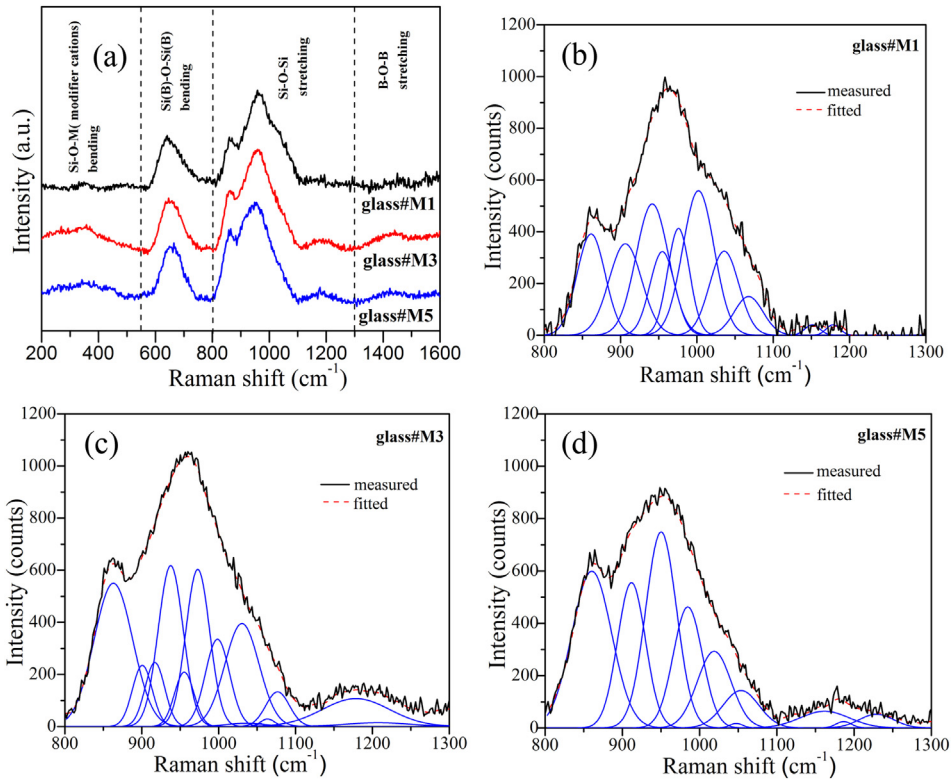

Fig. 5. (a) Raman spectra of quenched glasses, (b–d) deconvoluted spectra of glasses for glass#M1, glass#M3 and glass#M5, respectively.

confirms that the presence of MnO decreases the network connectivity of glass, consistent with the Raman results (in Fig. 5). It is well known fact that intermediate oxides like MnO_2, Cr_2O_3, TiO_2, Fe_2O_3 etc can act as a modifier or former depending on the initial glass compositions and their amounts [40].

Therefore, MnO (based on PL results in Fig. 2) acts a network modifier in glasses, which contributes to the decrease in network connectivity of glasses in present work. Park et al. also reported the network modifier effect of MnO on the network structure of CaO–MnO–SiO_2 glass (MnO ≤45 mol %) [37].

The glass transition temperature (T_g) of glasses decreased from 659 ± 3 °C for glass#M1 to 643 ± 3 °C for glass#M3 and to 631 ± 3 °C for glass#M5, as shown in Table 4. In addition, the softening temperature (T_d) of glasses decreases from 737 ± 3 °C for glass#M1 to 719 ± 3 °C for glass#M3 and to 701 ± 3 °C for glass#M5. It has been reported that the decrease in glass transition temperature and softening temperature often indicates a more open glass network [41,42]. The decreases in glass transition temperature and softening temperature with increasing MnO_2 dopant can thus be correlated to a more open glass network, in well agreement with decreasing network connectivity of glasses (in Fig. 6).

Table 3
Fractions of different [SiO_4] units in quenched glasses.

Sample ID	Q^0 (%)	Q^1 (%)	Q^2 (%)	Q^3 (%)	Q^4 (%)
Glass#M1	12	12	62	13	1
Glass#M3	20	10	57	7	6
Glass#M5	30	10	49	3	8

3.3. Glass/metal interfacial reaction

Fig. 7 shows the fraction of Cr^{6+} in the reaction couples between Cr_2O_3 and glass powers, after reacting in air at 600 °C, as a function of reaction time. It is worth noting that the maximum fraction of Cr^{6+} occurs in the reaction couple between Cr_2O_3 and glass#M3. For example, the fraction of Cr^{6+}, after reacting in air at 600 °C for 9 h, increases from 5.8% for glass#M1 to 7.9% for glass#M3 and then decreases to 4.6% for glass#M5. Considering the amorphous nature of glasses held in air at 600 °C for 9 h (in Fig. 1), the decreasing network connectivity of glasses with increasing MnO_2 dopant favors the interfacial reaction, because of the easier diffusion of Sr ion from glass to the interface. However, a more negative Gibbs free energy of the reaction, *i.e.*, $2MnO + 0.5O_2 = Mn_2O_3$, with greater MnO_2 dopant in glasses is more effective for the reduction of chromate phase, by consuming more oxygen available at the interface.

Fig. 8 shows the micrographs of glass–metal interfaces held at 700 °C for up to 500 h. The interfaces between glass#M3 and Crofer 22APU held at 700 °C for 100 and 500 h are selected for comparison, as shown in Fig. 8(a) and (b). It is clear that a gray layer formed at the glass/metal interface, which is identified to be Mn–Cr oxide by EDS elemental analysis. The diffraction peaks corresponding for Mn_2O_3 and Mn_3O_4 can be observed in the XRD patterns of the glass–ceramics held at 700 °C to 500 h (in Fig. 9), which indicates the presences of Mn^{2+} and Mn^{3+} ions in glass–ceramics. Therefore, the Mn–Cr oxide scale observed at the glass/metal interface in present work can be attributed to the segregations of Mn from the glass and Cr from the metal.

In addition, an EDS elemental line scan across the interface was performed in a magnified image of Fig. 8(b), as shown in Fig. 8(c). It is worth noting that the presence of Mn–Cr oxide layer prevents

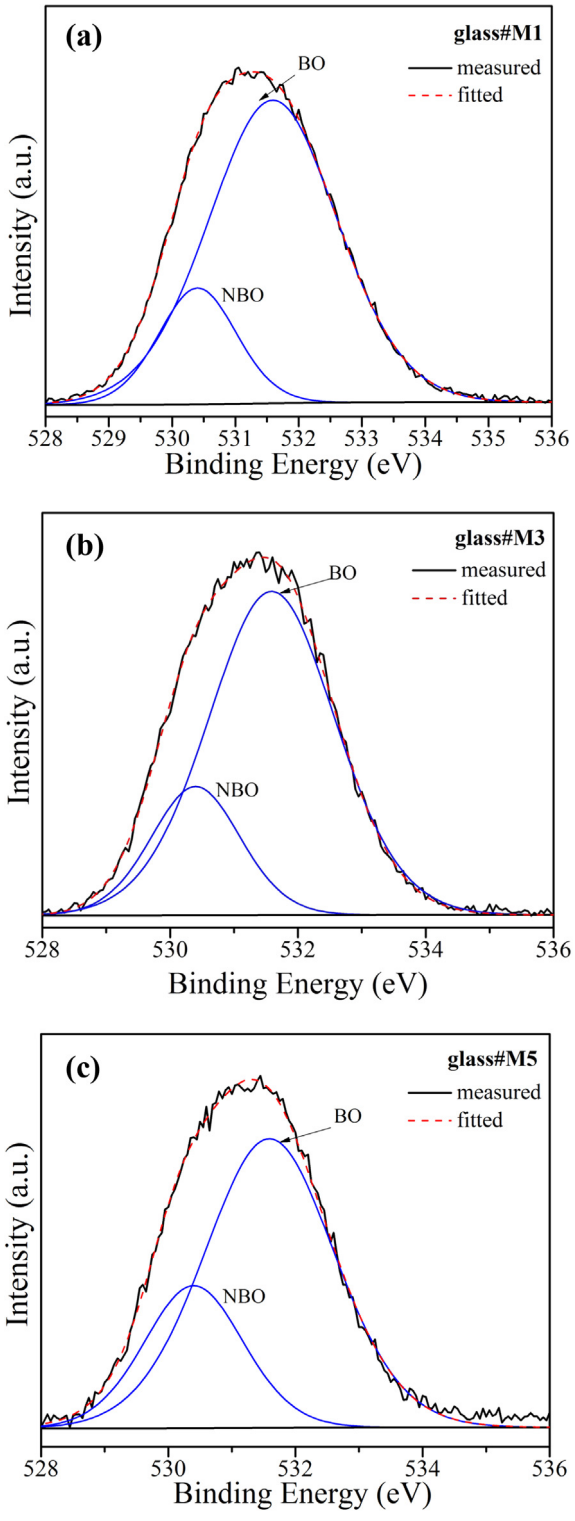

Fig. 6. O 1s spectra of quenched glasses for (a) glass#M1, (b) glass#M3, and (c) glass#M5.

the further diffusion of Cr from metallic interconnect to glass and therefore reduces the formation of chromate phase at the interface.

The spinel coatings, *e.g.*, $MnCo_2O_4$ [20], $Mn_{1.5}Co_{1.5}O_4$ [17,18] and $(Mn,Co)_3O_4$, [16,43] are often applied to the surface of the interconnects to hinder the diffusion [17]and evaporation [20,21] of Cr from the interconnects. However, Mahapatra et al. reported the

Table 4
Thermal properties of quenched glasses.

Sample ID	T_g (°C)	T_d (°C)	T_c (°C)	CTE ($\times 10^{-6}$ K^{-1}, 200–600 °C)
Glass#M1	659 ± 3	737 ± 3	790 ± 3	13.28 ± 0.03
Glass#M2	657 ± 3	724 ± 3	779 ± 3	13.62 ± 0.03
Glass#M3	643 ± 3	719 ± 3	775 ± 3	13.61 ± 0.03
Glass#M4	638 ± 3	711 ± 3	772 ± 3	13.62 ± 0.03
Glass#M5	631 ± 3	701 ± 3	771 ± 3	13.67 ± 0.03

T_c: onset crystallization temperature.
T_g: glass transition temperature.
T_d: dilatometric softening temperature.
CTE: coefficient of thermal expansion.

severe reaction between instable $(Mn,Co)_3O_4$ spinel coating and sealing glass, which led to the degradation of the interfacial compatibility [43]. In addition, Chou et al. found that the continuous spinel layer was broken into particles and islands by the reaction between spinel layer and the sealing glass, resulting in the structural degradation at the sealing interface [18]. It is also worth noting that the continuous Mn–Cr oxide scale with a thickness of about 3 μm can be observed at the interface between glass#M3 and Crofer 22APU held at 700 °C for up to 500 h (in Fig. 8).

Therefore, the competitive reaction reduces the redox chromate formation by consuming the oxygen at the glass/metal interface during the operation of SOFC (in Fig. 7). In addition, the competitive reaction contributes to the formation of a continuous Mn–Cr oxide scale at the glass/metal interface, which appears to be helpful for reducing the further diffusion of Cr from metallic interconnect to glass (in Fig. 8).

4. Conclusions

In present work, the effect of competitive reaction on the redox interfacial reaction has been clearly demonstrated in the reaction couples between Mn-containing glasses and Cr_2O_3 powers as well as the sealing couples between glasses and Crofer 22APU. The competitive reaction reduces the chromate formation by consuming the oxygen at the glass/metal interface. In addition, the competitive reaction contributes to the formation of a continuous Mn–Cr oxide scale at the glass/metal interface, which results in the good bondage between glass and metal. The redox glass/metal interfacial reaction can therefore be controlled by the introduction of competitive reaction. The finding on the control of redox glass/

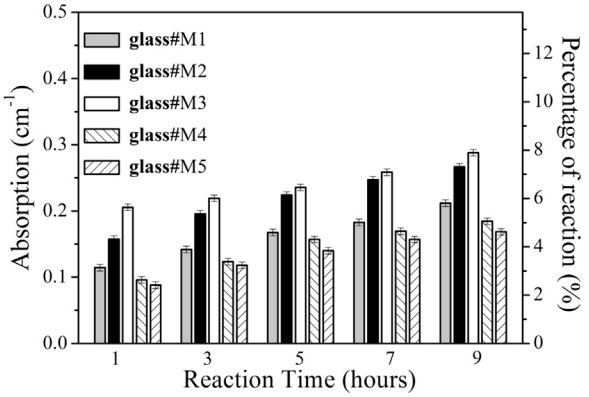

Fig. 7. The fraction of Cr^{6+} in the reaction couples between Cr_2O_3 and glass powders, after reacting in air at 600 °C for different times.

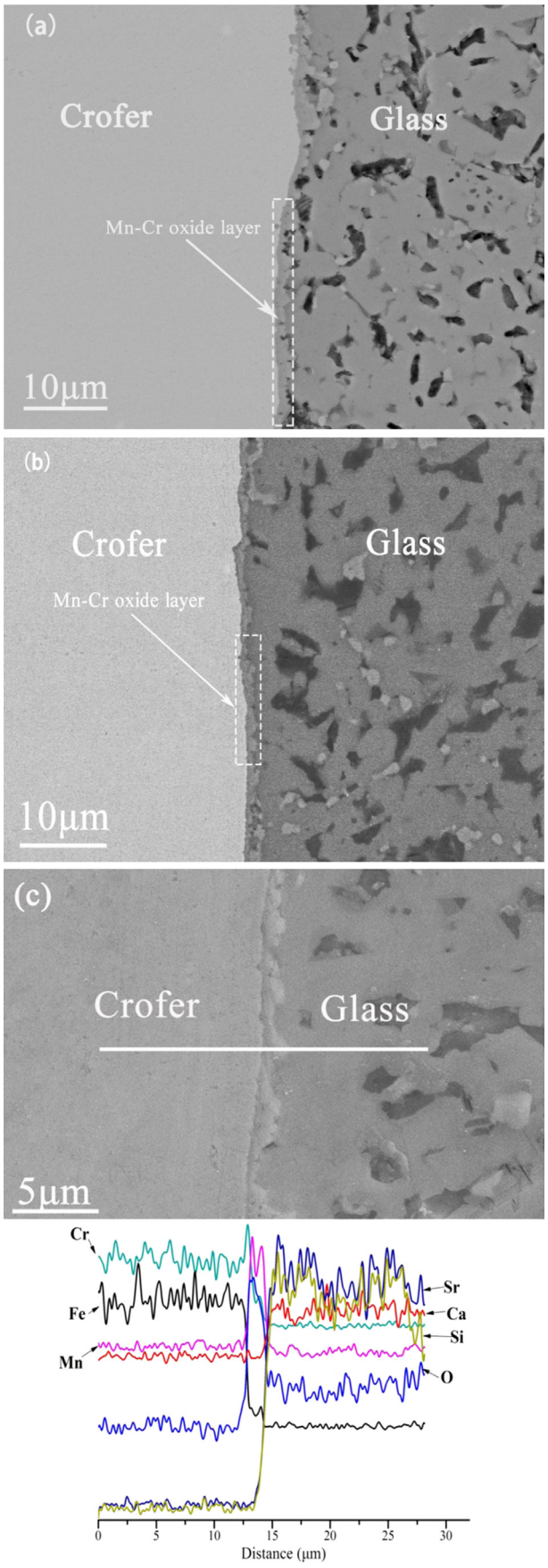

Fig. 8. Micrographs of the interface between glass#M3 and Crofer 22APU held at 700 °C for (a) 100 h, (b) 500 h, and (c) the magnified image in (b) and EDS elemental line scans across the interface.

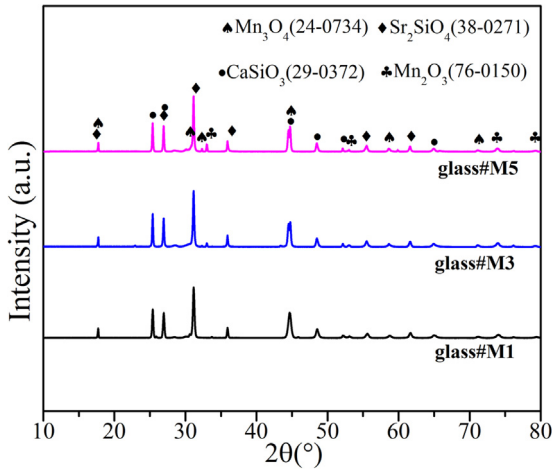

Fig. 9. XRD patterns of glass–ceramics held at 700 °C for 500 h.

metal interfacial reaction will shed lights onto the design of reliable sealing glasses for IT-SOFC application.

Acknowledgments

The authors gratefully acknowledge the financial support of the National Natural Science Foundation of China (No. 51102045), Program for New Century Excellent Talents in Fujian Province University (No. JA12013), funds for Distinguished Young Scientists from the Fujian Education Department (No. JA11007), and the National Undergraduate Innovative Experiment Program (No. 201310386021). They would also like to thank Zhenhuan Zheng for assistance with SEM/EDS, Qingming Huang for assistance with X-ray diffraction, Fen Lin for assistance with DSC analysis and Yunlong Yu for assistance with dilatometric measurement.

References

[1] M.K. Mahapatra, K. Lu, Mater. Sci. Eng. R: Rep. 67 (2010) 65–85.
[2] M.K. Mahapatra, K. Lu, J. Power Sources 195 (2010) 7129–7139.
[3] D.U. Tulyaganov, A.A. Reddy, V.V. Kharton, J.M.F. Ferreira, J. Power Sources 242 (2013) 486–502.
[4] Z. Yang, K.D. Meinhardt, J.W. Stevenson, J. Electrochem. Soc. 150 (2003) A1095–A1101.
[5] Y.S. Chou, E.C. Thomsen, R.T. Williams, J.P. Choi, N.L. Canfield, J.F. Bonnett, J.W. Stevenson, A. Shyam, E. Lara-Curzio, J. Power Sources 196 (2011) 2709–2716.
[6] G. Kaur, O.P. Pandey, K. Singh, Int. J. Hydrogen Energy 37 (2012) 6862–6874.
[7] T. Zhang, R.K. Brow, W.G. Fahrenholtz, S.T. Reis, J. Power Sources 205 (2012) 301–306.
[8] Y.S. Chou, J.W. Stevenson, J.P. Choi, J. Power Sources 250 (2014) 166–173.
[9] Y.S. Chou, J.W. Stevenson, P. Singh, J. Power Sources 184 (2008) 238–244.
[10] F. Smeacetto, M. Salvo, M. Ferraris, J. Cho, A.R. Boccaccini, J. Eur. Ceram. Soc. 28 (2008) 61–68.
[11] B. Kuhn, E. Wessel, J. Malzbender, R.W. Steinbrech, L. Singheiser, Int. J. Hydrogen Energy 35 (2010) 9158–9165.
[12] C.K. Lin, J.Y. Chen, J.W. Tian, L.K. Chiang, S.H. Wu, J. Power Sources 205 (2012) 307–317.
[13] J.H. Hsu, C.W. Kim, R.K. Brow, J. Power Sources 250 (2014) 236–241.
[14] Y.S. Chou, J.W. Stevenson, P. Singh, J. Power Sources 185 (2008) 1001–1008.
[15] J.P. Choi, K. Scott Weil, Y. Matt Chou, J.W. Stevenson, Z. Gary Yang, Int. J. Hydrogen Energy 36 (2011) 4549–4556.
[16] C.C. Mardare, H. Asteman, M. Spiegel, A. Savan, A. Ludwig, Appl. Surf. Sci. 255 (2008) 1850–1859.
[17] S.J. Widgeon, E.L. Corral, M.N. Spilde, R.E. Loehman, J. Am. Ceram. Soc. 92 (2009) 781–786.
[18] Y.S. Chou, J.W. Stevenson, G.G. Xia, Z.G. Yang, J. Power Sources 195 (2010) 5666–5673.
[19] M.K. Mahapatra, K. Lu, Int. J. Hydrogen Energy 35 (2010) 11908–11917.
[20] T. Uehara, N. Yasuda, M. Okamoto, Y. Baba, J. Power Sources 196 (2011) 7251–7256.
[21] R. Sachitanand, M. Sattari, J.-E. Svensson, J. Froitzheim, Int. J. Hydrogen Energy 38 (2013) 15328–15334.

[22] T. Zhang, Q. Zou, F. Zeng, S. Wang, D. Tang, H. Yang, J. Power Sources 216 (2012) 1–4.
[23] T. Zhang, H. Zhang, G. Li, H. Yung, J. Power Sources 195 (2010) 6795–6797.
[24] B. Sumalatha, I. Omkaram, T. Rajavardhana Rao, C. Linga Raju, Phys. B – Condens. Matter 411 (2013) 99–105.
[25] I. Ardelean, M. Peteanu, V. Simon, S. Filip, M. Flora, S. Simon, J. Mater. Sci. 34 (1999) 6063–6068.
[26] I.E.C. Machado, L. Prado, L. Gomes, J.M. Prison, J.R. Martinelli, J. Non-Cryst. Solids 348 (2004) 113–117.
[27] M. Oku, K. Hirokawa, S. Ikeda, J. Electron Spectrosc. Relat. Phenom. 7 (1975) 465–473.
[28] H.W.N.A.D. Baneree, Am. Mineral. 83 (1998) 305–315.
[29] M.C. Biesinger, B.P. Payne, A.P. Grosvenor, L.W.M. Lau, A.R. Gerson, R.S.C. Smart, Appl. Surf. Sci. 257 (2011) 2717–2730.
[30] S.P. Best, R.J.H. Clark, C.L. Hayward, R. Withnall, J. Raman Spectrosc. 25 (1994) 557–563.
[31] D.A. McKeown, I.S. Muller, A.C. Buechele, I.L. Pegg, C.A. Kendziora, J. Non-Cryst. Solids 262 (2000) 126–134.
[32] M.K. Mahapatra, K. Lu, R.J. Bodnar, Appl. Phys. A 95 (2009) 493–500.
[33] K. Lu, M.K. Mahapatra, J. Appl. Phys. 104 (2008) 074910–074919.
[34] M. Lenoir, A. Grandjean, S. Poissonnet, D.R. Neuville, J. Non-Cryst. Solids 355 (2009) 1468–1473.
[35] B.H.W.S. De Jong, C.M. Schramm, V.E. Parziale, J. Am. Chem. Soc. 106 (1984) 4396–4402.
[36] B. Mysen, P. Richet, Silicate Glasses and Melts: Properties and Structure, Elsevier Science, 2005.
[37] J.H. Park, J. Non-Cryst. Solids 358 (2012) 3096–3102.
[38] Y. Miura, H. Kusano, T. Nanba, S. Matsumoto, J. Non-Cryst. Solids 290 (2001) 1–14.
[39] C. Yusufali, R.J. Kshirsagar, Jagannath, R.K. Mishra, R.S. Dutta, G.K. Dey, J. Non-Cryst. Solids 366 (2013) 54–58.
[40] A. Arora, V. Kumar, K. Singh, O.P. Pandey, Ceram. Int. 37 (2011) 2101–2107.
[41] R.F. Cuevas, A.M. de Paula, O.L. Alves, N. Aranha, J.A. Sanjurjo, C.L. Cesar, L.C. Barbosa, J. Mater. Chem. 6 (1996) 1811–1814.
[42] P. Pascuta, M. Bosca, G. Borodi, E. Culea, J. Alloys Compd. 509 (2011) 4314–4319.
[43] M.K. Mahapatra, K. Lu, J. Power Sources 196 (2011) 700–708.